Report

SOURCE DATA | TRANSPARENT PROCESS | OPEN ACCESS

EMBO reports

# Conformational change of *Plasmodium* TRAP is essential for sporozoite migration and transmission

Friedrich Braumann[1,†], Dennis Klug[1,2,*,†], Jessica Kehrer[1,3], Gaojie Song[4,5], Juan Feng[4], Timothy A Springer[4,**] & Friedrich Frischknecht[1,3,***]

## Abstract

**Eukaryotic cell adhesion and migration rely on surface adhesins connecting extracellular ligands to the intracellular actin cytoskeleton. *Plasmodium* sporozoites are transmitted by mosquitoes and rely on adhesion and gliding motility to colonize the salivary glands and to reach the liver after transmission. During gliding, the essential sporozoite adhesin TRAP engages actin filaments in the cytoplasm of the parasite, while binding ligands on the substrate through its inserted (I) domain. Crystal structures of TRAP from different *Plasmodium* species reveal the I domain in closed and open conformations. Here, we probe the importance of these two conformational states by generating parasites expressing versions of TRAP with the I domain stabilized in either the open or closed state with disulfide bonds. Strikingly, both mutations impact sporozoite gliding, mosquito salivary gland entry, and transmission. Absence of gliding in sporozoites expressing the open TRAP I domain can be partially rescued by adding a reducing agent. This suggests that dynamic conformational change is required for ligand binding, gliding motility, and organ invasion and hence sporozoite transmission from mosquito to mammal.**

**Keywords** adhesin; cell migration; gliding motility; integrins; malaria
**Subject Categories** Cell Adhesion, Polarity & Cytoskeleton; Microbiology, Virology & Host Pathogen Interaction; Structural Biology
**DOI** 10.15252/embr.202357064 | Received 25 February 2023 | Revised 15 May 2023 | Accepted 16 May 2023
**EMBO Reports (2023) e57064**

## Introduction

Malaria-causing parasites undergo a complex life cycle between mosquitoes and vertebrate hosts. A key feature, essential during transmission to and from the mosquito, is parasite motility (Douglas *et al*, 2015). *Plasmodium* sporozoites develop in oocysts at the midgut wall and egress into the circulating fluid of the hemolymph followed by specific emigration into salivary glands (Frischknecht & Matuschewski, 2017). Within the salivary glands, sporozoites mature and gain the capacity to be highly motile once isolated or transmitted (Vanderberg, 1974). During the probing phase of a mosquito bite, the sporozoites are ejected with the saliva into the skin, where they migrate at high speed and enter into lymph and blood vessels (Menard *et al*, 2013; Hopp *et al*, 2021). Those entering the bloodstream are transported throughout the circulatory system and arrest specifically in the liver, where they ultimately enter hepatocytes to differentiate into merozoites, which subsequently infect red blood cells (Prudencio *et al*, 2006).

To navigate this complex journey (Fig 1A), sporozoites have a number of surface proteins including the single-pass transmembrane adhesin termed thrombospondin-related anonymous protein (TRAP). TRAP likely evolved to bind multiple ligands found in the salivary gland, skin, and liver (Matuschewski *et al*, 2002; Klug *et al*, 2020). TRAP harbors two extracellular domains, the inserted (I) domain and the thrombospondin type I repeat, TSR. On the cytoplasmic side, a small tail links to actin filaments that are formed underneath the plasma membrane (Heintzelman, 2015; Fig 1B). The I domain is found in many other proteins, including integrins of multicellular organisms. Deletion of *trap* allows sporozoite formation and exit from the oocysts, but *trap(−)* parasites largely fail to enter the salivary glands (Sultan *et al*, 1997). Hemolymph-derived *trap(−)* sporozoites also show defects in substrate adhesion, fail to undergo typical gliding motility (Fig 1C), and instead can only move back and forth over a single adhesion site, a phenomenon termed patch gliding (Münter *et al*, 2009). Deletion of the I domain largely phenocopies deletion of the entire protein, and mutations in or around the metal ion-dependent adhesion site (MIDAS) compromise sporozoite infectivity (Matuschewski *et al*, 2002; Klug *et al*, 2020).

Crystal structures of the N-terminal portion of TRAP containing the TSR and I domain in human-infective *Plasmodium* spp. revealed

1 Integrative Parasitology, Center for Infectious Diseases, Heidelberg University Medical School, Heidelberg, Germany
2 Université de Strasbourg, CNRS UPR9022, INSERM U963, Institut de Biologie Moléculaire et Cellulaire, Strasbourg, France
3 German Center for Infection Research, Partner Site Heidelberg, Heidelberg, Germany
4 Program in Cellular and Molecular Medicine, Children's Hospital Boston, and Departments of Biological Chemistry and Molecular Pharmacology and of Medicine, Harvard Medical School, Boston, MA, USA
5 Department of Biology, East China Normal University, Shanghai, China
*Corresponding author. Tel: +49 152 18422189; E-mail: dennis.klug@sciencebridge.net
**Corresponding author. Tel: +1 617 713 8200; E-mail: springer@crystal.harvard.edu
***Corresponding author. Tel: +49 6221 566537; Fax: +49 6221 564643; E-mail: freddy.frischknecht@med.uni-heidelberg.de
†These authors contributed equally to this work

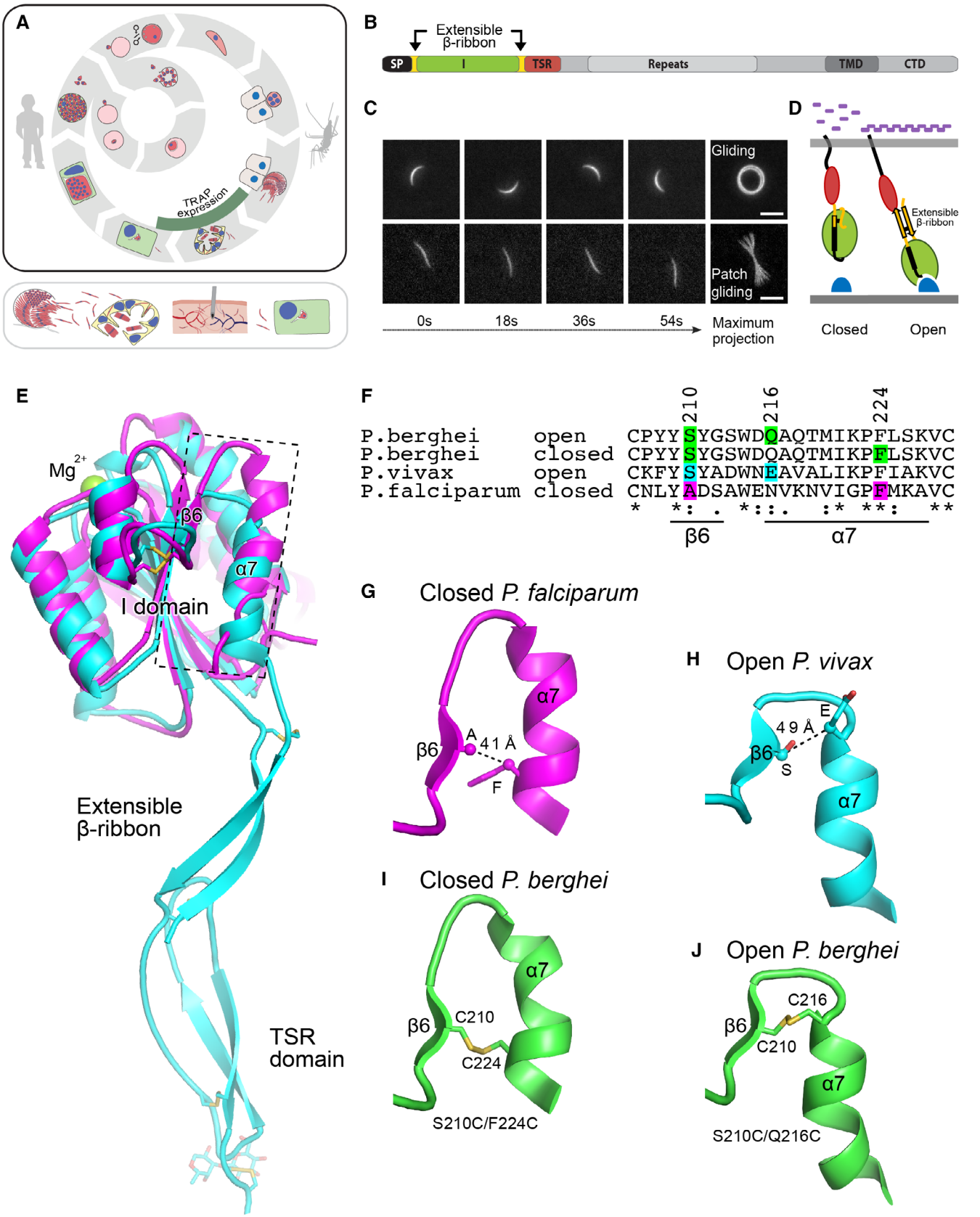


**Figure 1.**

**Figure 1. TRAP mediated sporozoite migration and I domain conformation.**

A A simplified schematic overview of the *Plasmodium* life cycle. Upper box: The part of the life cycle in which TRAP is expressed is highlighted with a green arc. Lower box: sporozoites egress from oocysts and actively enter salivary glands, cross through the dermis and enter hepatocytes.

B Domains in full-length TRAP showing signal peptide (SP), I domain (I, green), extensible β-ribbon (yellow), thrombospondin type I repeat (TSR), disordered repeats, transmembrane domain (TMD), and cytoplasmic tail domain (CTD).

C Movie stills (first four panels in each row) and maximum intensity projections (5$^{th}$ panel in each row) from a 90-s video of *P. berghei* sporozoites undergoing normal circular gliding motility (top row) and patch gliding (bottom row). Scale bars: 5 μm.

D Schematic of TRAP linkage to the cytoskeleton and ligand binding. TRAP I domain (green) is hypothesized to be primarily in the closed conformation when unbound, with low adhesion and no signaling activity. TRAP I domain is hypothesized to be primarily in the open conformation when bound to substrate ligands (blue), potentially leading to intracellular signaling and interaction with actin filaments (lilac). Red: TSR; yellow: extensible ribbon as in Fig 1B.

E *P. falciparum* (closed) and *P. vivax* (open) TRAP crystal structures (ribbon cartoons in cyan and magenta, respectively) aligned on the I domain (Song *et al*, 2012). The extensible β-ribbon and TSR domain were ordered (visualized) only in the open structure). The boxed area is shown in detail in panels (G) and (H).

F Sequence alignment of the C-terminal portion of TRAP I domains. Residues highlighted in bottom two rows are shown in stick in panels (G) and (H) and were used to predict locations of residues highlighted in top two rows for mutations to cysteine.

G, H Details of boxed region in (E) with sidechains in optimal positions for mutation to cysteine with dashed lines between Cβ atom positions with distances marked. The structural alignment is maintained horizontally in the figure, note that the β6-strands are in similar positions, while the β6-α7 loop and α7-helix are shifted.

I, J Alphafold predictions of *P. berghei* TRAP I domain cysteine mutants were structurally superimposed on the I domains with crystal structures shown in panel (E); details are shown for the same portions as in panels (G) and (H). Notably, cysteine disulfide bonds form and the conformation of the β6 and α7 segment is essentially identical to that of the closed and open crystal structure segments shown above in (G) and (H), respectively.

Source data are available online for this figure.

the I domain in both open and closed conformations (Song *et al*, 2012; Fig 1D and E). Mammalian integrin I domains and TRAP I domains undergo structurally homologous conformational changes between open and closed conformations (Shimaoka *et al*, 2002; Song *et al*, 2012). Reshaping occurs in loops that surround a metal ion-dependent adhesion site (MIDAS), which holds a $Mg^{2+}$ that coordinates an acidic residue in ligands at the center of the ligand binding site. Mammalian open and closed I domains have high and low affinity for ligand, respectively (Shimaoka *et al*, 2002). Alteration around the ligand binding site in the I domain is linked to pistoning of its α7-helix such that in the open state of TRAP an extensible β-ribbon appears between the I and TSR domains (Fig 1D and E). Binding to ligand is expected to stabilize the putative high affinity, open conformation of the TRAP I domain. Force applied by the actin cytoskeleton to TRAP that is resisted by extracellular ligand would transmit tensile force through TRAP and further stabilize its extended, open conformation with the extensible β-ribbon. A similar force-dependent process stabilizes the extended, open conformation of integrins (Li & Springer, 2017). Hence, ligand binding, together with tensile force, likely stabilizes a strong conformational change in TRAP during gliding motility. In integrins, stabilizing the domain in an open state by engineered disulfide bonds increased ligand affinity ~ 1,000-fold (Shimaoka *et al*, 2001).

To investigate whether the two TRAP I domain conformational states are also important for sporozoite migration and infectivity, we designed cysteine mutations that would form disulfide bonds to stabilize closed and open conformations of the *Plasmodium berghei* TRAP I domain. Both mutations impacted the capacity of sporozoites to migrate, enter salivary glands, and infect mice. Interestingly, hemolymph-derived sporozoites expressing the open conformation could not migrate on flat surfaces but still entered into salivary glands, albeit at a reduced level compared with wild-type. Sporozoites derived from the salivary gland remained immotile, but their motility could be partly rescued by the addition of the reducing agent dithiothreitol (DTT). Our results suggest that active change between the open and closed conformation of the TRAP I domain is essential for sporozoite invasion of salivary glands and transmission from mosquitoes to mammals.

## Results and Discussion

### *P. berghei* sporozoites expressing TRAP with conformationally stabilized I domains fail to transmit

We used closed and open structures of TRAP from *P. falciparum* and *P. vivax*, respectively (Song *et al*, 2012), to design cysteine mutations in *P. berghei* (Fig 1E–J). The TRAP I domain of *P. berghei* is 42 and 48% identical in sequence to those of *P. vivax* and *P. falciparum*, respectively; lower identity was used for successful introduction of a disulfide into integrin αI domains (Shimaoka *et al*, 2001, 2003). Between the open and closed TRAP I domain conformations, the I domain α7-helix pistons 9 Å relative to the neighboring β6-strand; therefore, disulfides introduced between these two structural elements can stabilize one state over the other, as previously pioneered in integrin I domains. β6-strand and α7-helix residues with Cβ atoms within 5 Å of one another in structures of the two states were chosen for mutation to cysteine (Fig 1F–H). *P. falciparum* TRAP-Fc fusions with homologous cysteine mutations were well expressed in mammalian cells (Song *et al*, 2012). Using the TRAP sequence alignment (Fig 1F), homologous residues in *P. berghei* TRAP were mutated to cysteine to stabilize the closed conformation (Ser-210 and Phe-224 in the S210C/F224C mutation) and the open conformation (Ser-210 and Gln-216 in the S210C/Q216C mutation). AlphaFold (Mirdita *et al*, 2022) predicted that the *P. berghei* TRAP I domains were well folded, assumed the desired conformations, and that the mutationally introduced disulfide bonds formed and were in very high confidence regions (Figs 1I and J and EV1A–D). The I domain of *P. berghei* is 42 and 48% identical in sequence to those of *P. vivax* and *P. falciparum* in which the open and closed conformations are defined, assuring highly confident modeling (Song *et al*, 2012). Cysteines were substituted in positions that were sufficiently close in one conformation to form a disulfide but not in the alternative

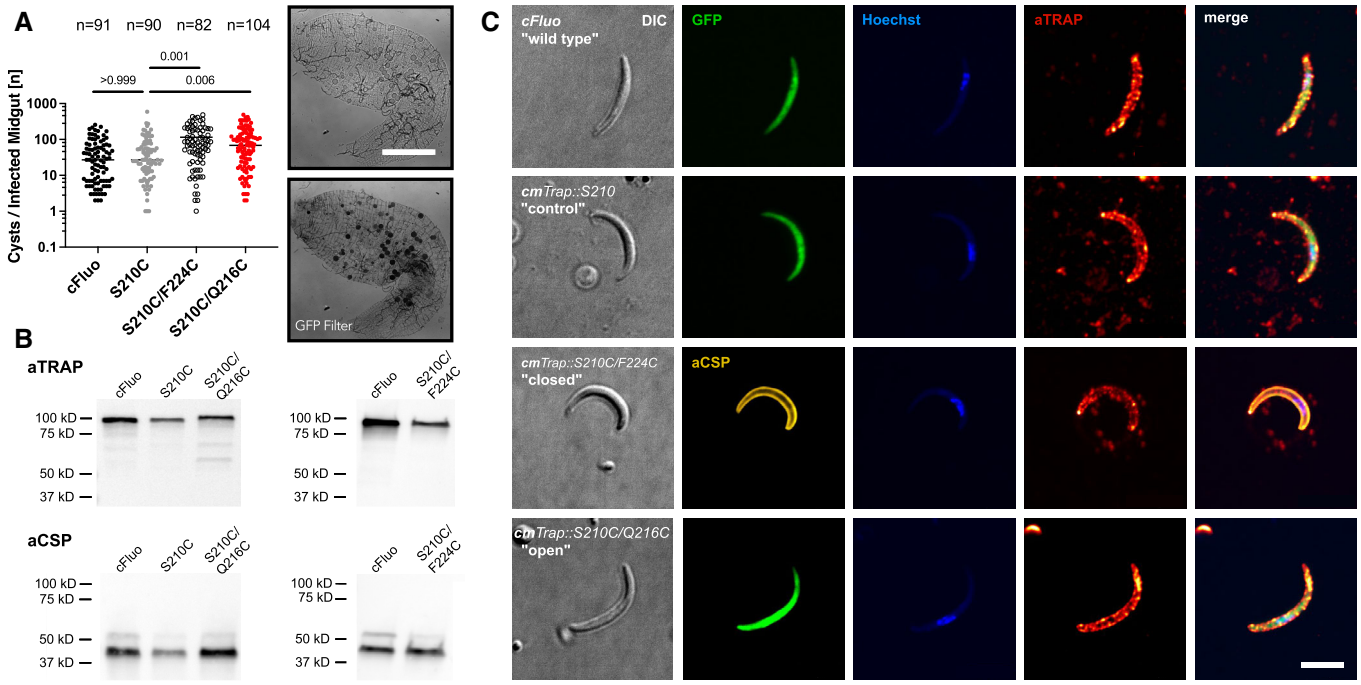


**Figure 2. Modified TRAP proteins are expressed and localized as in wild type controls.**

A Numbers of oocysts in infected midguts of the different lines. Values (*n*) above dot plots indicate numbers of observed midguts. Shown are data from three biological replicates. Numbers above horizontal bars indicate *P*-values. Data were tested for significance using the Kruskal–Wallis test. Images show *cFluo* oocysts in an infected midgut without (top) and with (bottom) green fluorescence. Scale bar: 200 µm.

B Western blots using an anti-TRAP antibody of the control lines *cFluo* and *S210C* in comparison with *S210C/Q216C* (open) and *S210C/F224C* (closed). Anti-CSP antibody mAb 3D11 was used as loading control, revealing the two expected CSP bands (Coppi *et al*, 2011).

C Surface expression of TRAP mutants on fixed but not permeabilized sporozoites. Differential interference contrast (DIC) and immunofluorescence images of representative examples of hemolymph-derived sporozoites of the indicated parasite lines stained with anti-TRAP antibodies shown in red (Klug *et al*, 2020). Hoechst was used to reveal the sporozoite nuclear DNA shown in blue. Cytoplasmic GFP or staining with anti-CSP antibodies was used to validate the integrity of sporozoites. Scale bar: 5 µm.

Source data are available online for this figure.

conformation. These cysteine mutations were introduced into a codon-modified version of *trap*; a single S210C mutant was used as a control. These TRAP constructs were ligated into an existing vector (Klug *et al*, 2020) in order to replace the endogenous TRAP (Fig EV2A–D). Constructs were either transfected into the fluorescent line *cFluo*, expressing EGFP constitutively from the *ef1α* promoter and mCherry in insect stages from the *csp* promoter, or a nonfluorescent *trap(−)* line (Bane *et al*, 2016; Klug *et al*, 2020). Generation of clonal lines yielded the parasite lines *S210C* (control, fluorescent), *S210C/F224C* (closed, nonfluorescent), and *S210C/Q216C* (open, fluorescent). For all experiments, the *cFluo* line was used as the control and will be referred to as wild-type in the following. As expected, all lines showed no growth difference to wild-type parasites in mice. Also, all lines showed a similar range of mosquito infection with the numbers of oocysts even being increased for the closed and open mutants (Fig 2A). Sporozoites also egressed efficiently from oocysts and could be isolated from the hemolymph. Western blotting of hemolymph-derived sporozoites showed similar expression of TRAP in the wild-type, control, and conformationally stabilized parasite lines (Fig 2B). Immunofluorescence analysis of hemolymph-derived sporozoites that were fixed but not permeabilized revealed similar signals of TRAP on the surface in all lines (Fig 2C). The numbers of sporozoites were similar among all lines in the midgut (Fig 3A) but showed a dramatic drop in salivary gland residency of the lines expressing TRAP in the closed and open conformations (Fig 3B). As similar numbers across all lines were found in the hemolymph (Fig 3C), we concluded that there must be a defect in salivary gland invasion to explain the large drop in midgut vs salivary glands ratio (Fig 3D, Table 1).

To investigate the capacity to infect mice, we isolated sporozoites of all three lines as well as the wild-type from the hemolymph and injected 10,000 sporozoites of each line into individual naïve C57Bl/6 mice. This showed the expected 100% infection rate in wild-type and S210C control parasites with a prepatent period (time until parasites can be detected in red blood cells) of around 5 days (Fig 4A–C and Table 2). However, hemolymph sporozoites expressing the closed or open TRAP I domains infected only around 50% of mice and those infected showed a prolonged prepatent period of 6–7 days (Fig 4A–C and Table 2). We next determined how the decreased colonization of the salivary glands by the closed and open mutants affected transmission of sporozoites. To this end, we allowed 10 infected mosquitoes to bite a naïve mouse and determined the onset and development of a blood-stage infection. As expected, the two control lines (wild-type

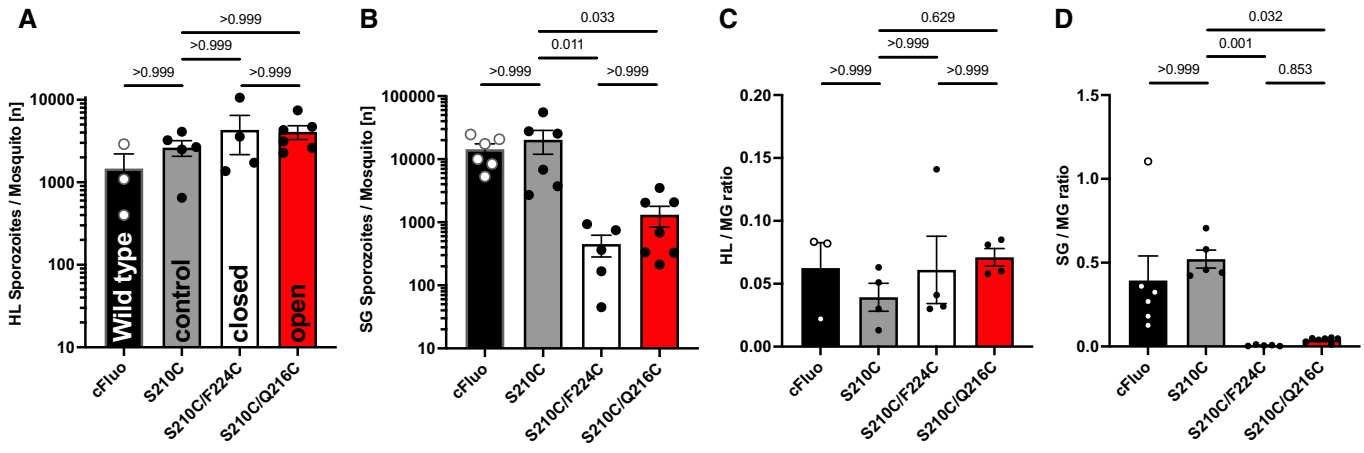


**Figure 3. Sporozoites with fixed I domains show strong reduction in salivary gland invasion.**

A Numbers of hemolymph (HL)-derived sporozoites reveal no difference between the parasite lines.

B Numbers of salivary gland (SG)-derived sporozoites reveal strong reduction in salivary gland invasion for the closed and open I domain expressing parasite lines.

C Ratios of hemolymph (HL)-derived versus oocyst-derived sporozoites reveal no difference between the parasite lines.

D Ratios of salivary gland (SG)-derived versus oocyst (MG)-derived sporozoites reveal strong reduction in salivary gland invasion for the closed and open I domain expressing parasite lines.

Data information: In (A–D), each condition represents pooled data from 3 to 7 biological replicates with dots representing data from individual mosquito feedings. Shown is mean ± SEM. Data were tested for significance with the Kruskal–Wallis test. Numbers above horizontal bars indicate *P*-values.
Source data are available online for this figure.

**Table 1. Absolute sporozoite numbers in midgut (MG), hemolymph (HL), and salivary glands (SG) of all analyzed parasite strains.**

| | No. of HL sporozoites | No. of MG sporozoites | No. of SG sporozoites | HL/MG ratio | SG/MG ratio | Mosquitoes with > 1,000 spz |
|---|---|---|---|---|---|---|
| cFluo | 1,500 ± 1,300 | 28,000 ± 20,000 | 14,000 ± 7,600 | 0.06 ± 0.04 | 0.39 ± 0.36 | 6/6 |
| S210C | 2,600 ± 1,300 | 57,000 ± 22,000 | 20,000 ± 20,000 | 0.04 ± 0.03 | 0.54 ± 0.13 | 6/6 |
| S210C/Q216C | 4,100 ± 1,700 | 52,000 ± 40,000 | **1,300 ± 1,300** | 0.07 ± 0.01 | **0.04 ± 0.01** | **3/7** |
| S210C/F224C | 4,300 ± 4,300 | 73,000 ± 32,000 | **450 ± 380** | 0.06 ± 0.05 | **0.01 ± 0.01** | **0/5** |

Last column shows countings from infected mosquito cages that revealed over 1,000 sporozoites per salivary gland (on average) from at least 10 dissected mosquitoes. Shown is mean ± SD. Bold numbers indicate significant difference from controls.

and S210C) infected all mice and showed prepatent periods of 3–4 days (Fig 4D–F and Table 2). In contrast, mosquitoes that were infected by the closed mutant (S210C/F224C) could not infect mice, while one out of 10 mice bitten by mosquitoes harboring the open mutant (S210C/Q216C) was infected (Fig 4D–F and Table 2). This mouse showed a delayed onset of blood-stage infection at 6-day post-infection. The number of salivary gland-derived sporozoites in the open mutant (S210C/Q216C) was not significantly higher than in the closed mutant (S210C/F224C; Fig 3C); however, we never managed to isolate sufficient numbers of sporozoites from salivary glands of the closed mutant (S210C/F224C) to conduct further experiments. We, therefore, isolated only sporozoites from salivary glands of mosquitoes infected by the control lines or the open mutant (S210C/Q216C) and injected these into naïve mice. This showed that three out of five mice infected with S210C/Q216C salivary gland sporozoites became blood-stage patent, albeit again with a 2-day delay compared with the controls, while all mice infected with the controls became blood-stage positive (Fig 4G–I and Table 2). This suggests that both mutants are severely impacted in their capacity to transmit from mosquitoes to mammals (Table 1).

## Conformationally stabilized open mutants do not glide

As gliding motility is a key factor in sporozoite infectivity, we next investigated the capacity of the control and mutant lines to glide in a standard gliding assay. To this end, sporozoites were either isolated from the hemolymph or salivary glands (if possible) and placed in RPMI medium containing 3% bovine serum albumin (BSA), which stimulates motility (Vanderberg, 1974). We scored the different patterns of motility that could be observed (Fig EV3). This analysis showed robust gliding motility for the control parasites isolated from both hemolymph or salivary glands, which was comparable to wild-type (Fig 5A and B). In contrast, hemolymph-derived sporozoites expressing TRAP in either the closed or open form showed strongly impaired gliding motility. Sporozoites expressing

the closed I domain (S210C/F224C) showed low levels of persistent gliding (~ 10% of control level). Strikingly, despite the observation of hundreds of sporozoites expressing the open I domain (S210C/Q216C), none of these were gliding (Fig 5A). This observation is somewhat counterintuitive since sporozoites expressing the open variant (S210C/Q216C) showed some level of colonization of the salivary glands (Fig 3A–D). Isolation of sporozoites expressing the open I domain (S210C/Q216C) from the salivary glands also showed no motility, while the controls moved as expected (Fig 5B). Interestingly, hemolymph sporozoites expressing the closed I domain

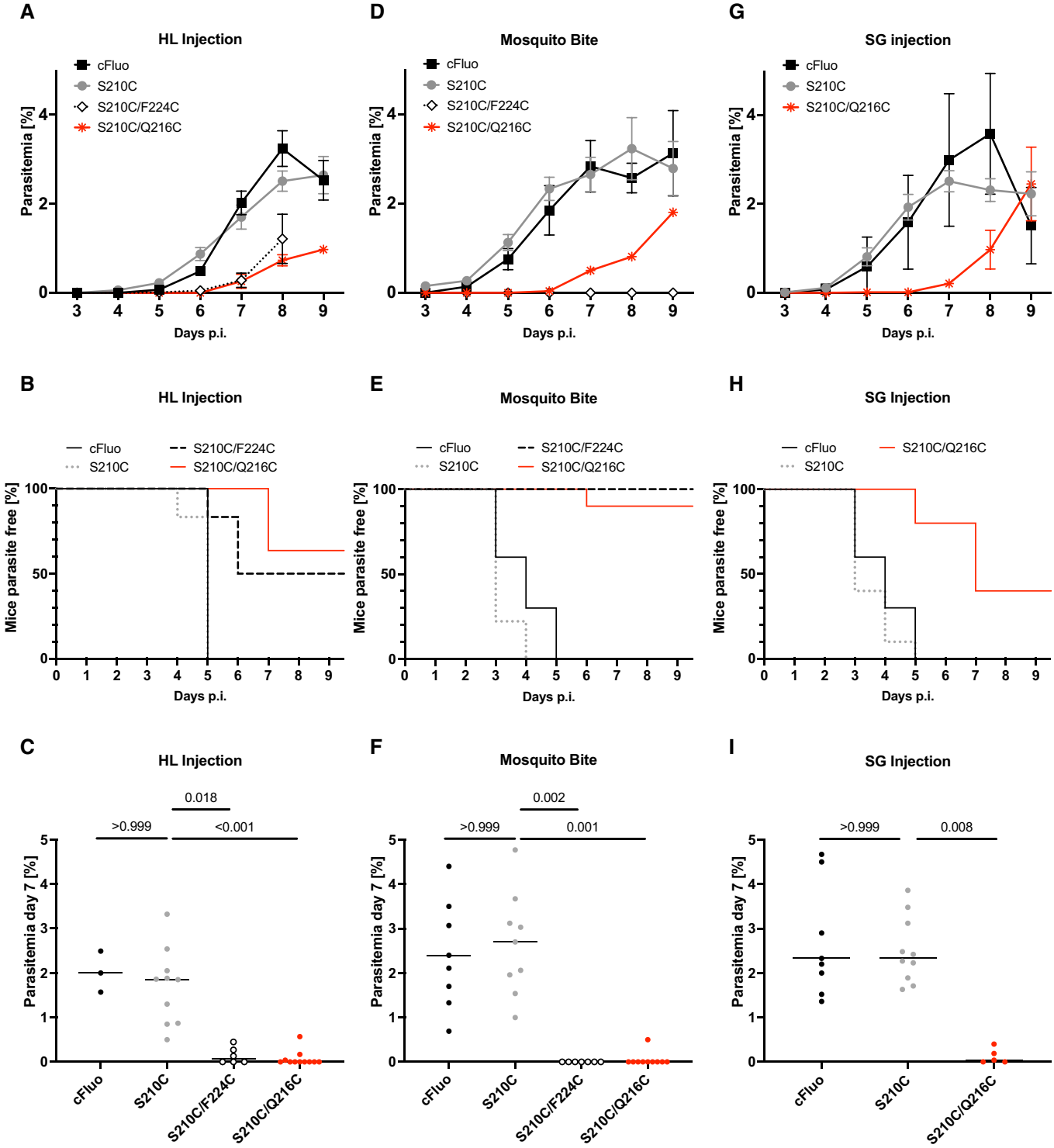


**Figure 4.**

**Figure 4. Conformational stabilization of the TRAP I domain impedes transmission.**

A Blood-stage parasitemia after injection of 10,000 hemolymph (HL)-derived sporozoites of the different lines into C57Bl/6 mice from Day 3 to Day 9 post infection. Shown is the mean ± SEM. Only data of infected mice have been plotted.

B Kaplan–Meier plot showing the percentage of parasite-free mice until Day 9 of infection.

C Parasitemia on Day 7 post hemolymph sporozoite (HLS) injection, tested for significance with Kruskal–Wallis test. Numbers above horizontal bars indicate *P*-values.

D Blood-stage parasitemia after C57Bl/6 mice were bitten by mosquitoes (10 mosquitoes/mouse) infected with the indicated parasite lines at Day 0. Shown is the mean ± SEM where appropriate. Only data of infected mice have been plotted for all but the S210C/F224C (closed I domain) infections, where all mice stayed negative.

E Kaplan–Meier plot showing the percentage of parasite-free mice after mosquito bites until Day 9 of infection.

F Parasitemia on Day 7 post mosquito bite, tested for significance with Kruskal–Wallis test. Numbers above horizontal bars indicate P-values.

G Blood-stage parasitemia after injection of 10,000 salivary gland (SG)-derived sporozoites of the indicated parasite lines into C57Bl/6 mice at Day 0. Shown is the mean ± SEM. Only data of infected mice have been plotted.

H Kaplan–Meier plot showing the percentage of parasite-free mice after salivary gland sporozoite injection until Day 9 of infection.

I Parasitemia on Day 7 post salivary gland sporozoite (SG) injection, tested for significance with Kruskal–Wallis test. Numbers above horizontal bars indicate *P*-values.

Data information: In (A–C), shown are pooled data from 3 (S210C), 2 (S210C/F224C), 3 (S210C/Q216C), and 1 (wild type) biological replicates using 3 or 4 mice, respectively. In (D–F), each condition represents pooled data from three biological replicates using 2–4 mice, respectively. In (G–I), shown are pooled data from 3 (S210C), 2 (S210C/Q216C) and 3 (wild type) biological replicates using 2–4 mice, respectively.
Source data are available online for this figure.

**Table 2. Transmission potential of the generated parasite lines *S210C*, *S210C/Q216C*, and *S210C/F224C* in comparison with the control *cFluo*.**

| Parasite line | Inoculation type | Mice infected/total exposed | Prepatency (days) |
|---|---|---|---|
| cFluo | HL iv | 3/3 | 5.0 |
| | SG iv | 10/10 | 3.9 |
| | Mosquito bite | 10/10 | 3.9 |
| S210C | HL iv | 10/10 | 4.8 |
| | SG iv | 10/10 | 3.5 |
| | Mosquito bite | 9/9 | 3.2 |
| S210C/F224C | HL iv | 3/6 | 5.7 |
| | SG iv | n.d. | n.d. |
| | Mosquito bite | 0/10 | n.a. |
| S210C/Q216C | HL iv | 3/11 | 7.0 |
| | SG iv | 3/5 | 6.3 |
| | Mosquito bite | 1/10 | 6.0 |

The prepatency is determined as the time between infection and the first observance of blood stages and is given as the mean of all mice that became blood stage positive; n.d., not determined, n.a., not applicable.

(S210C/F224C) showed more floating parasites suggesting reduced adhesion (Fig 5A). Intriguingly, the few moving sporozoites of this mutant were significantly faster during migration than corresponding controls (Fig 5C). This hints at a decrease in adhesion capacity of the closed mutant, which initially speeds up parasites but also reduces their capacity to stay attached to the substrate, as observed before for sporozoites treated with drugs that affect actin polymerization (Münter *et al*, 2009).

### A reducing agent rescues motility in TRAP open I domain expressing sporozoites

Disulfide bonds can be opened by a reducing agent. Hence, we hypothesized that adding reducing agents to the medium might reconstitute motility of sporozoites expressing the open I domain (S210C/Q216C). However, there are other structurally important disulfide bonds present in TRAP as well as in other proteins on the sporozoite surface, including the circumsporozoite protein (CSP), the major surface protein of sporozoites (Doud *et al*, 2012). Nevertheless, we aimed to find a condition, in which the advantage gained by disrupting our introduced disulfide bonds outweighs the disruption of other disulfide bonds. To increase the likelihood of finding an ideal experimental setup, we tested two reducing agents, dithiothreitol (DTT) and tris(2-carboxyethyl)phosphine (TCEP), which differ in their ability to cross membranes and, because of structural differences, in their potential to reduce disulfide bonds in folded proteins (Cline *et al*, 2004). We screened a range of DTT and TCEP concentrations and incubation times. By doing so, we found that gliding assays could not be performed in the simultaneous presence of BSA and reducing agents, as amorphous aggregates formed (Yang *et al*, 2015). Instead, we incubated sporozoites with DTT or TCEP before starting the actual assay. The reducing agents were then washed out, and the sporozoites were activated with RPMI medium supplemented with 3% BSA. Notably, this prolonged protocol resulted in a reduction of approximately 60% in productively moving wild-type sporozoites which has to be taken into account when comparing results from regular gliding assays with assays performed with DTT and TCEP-treated sporozoites (Fig 5D). We first determined at which concentration of DTT or TCEP, wild-type sporozoites were still motile (Table 3). This showed that already after 15-min incubation, a significant reduction of motility could be observed at 50 mM of DTT and at 5 mM of TCEP. At concentrations of 300 mM DTT and 50 mM TCEP, respectively, no motility was observed anymore (Figs 5D and EV4, Table 3). We, therefore, incubated hemolymph-derived sporozoites expressing the open I domain (S210C/Q216C) in different low concentrations of DTT and TCEP. Gliding assays under reducing conditions were only performed with sporozoites expressing TRAP fixed in the open state (S210C/Q216C) as sporozoites of this mutant showed no productive gliding under regular conditions. Gliding assays with reducing agents revealed conditions in which DTT could rescue motility of sporozoites expressing the open I domain (S210C/Q216C; Table 4). At 50 and 100 mM, 3 and 1.5% of sporozoites were found productively moving, respectively (Figs 5E and F and EV4A–D). This compares to 13% of control parasites moving in the absence of DTT and 10 and 7.4% moving at 50 and 100 mM DTT, respectively (Fig 5D). Hence,

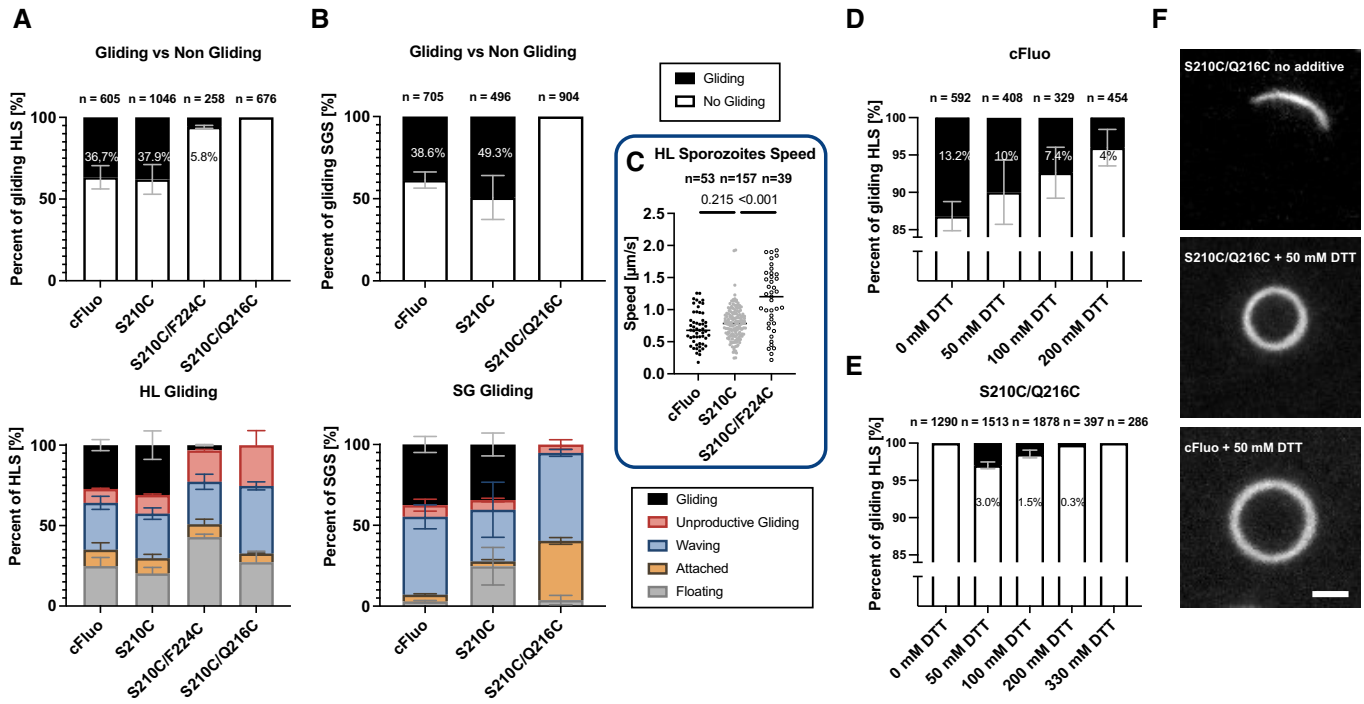


**Figure 5. Sporozoites expressing the open TRAP I domain do not glide unless treated with DTT.**

A Movement type analysis of hemolymph-derived sporozoites (HLS) of the indicated parasite lines. Top: Classification of attached sporozoites by motility. Bottom: Classification by motility type. *n* indicates the number of observed sporozoites. See Fig EV3 for the classification of different movement patterns. Floaters have been omitted in the analysis presented in the top graph and are not included in *n*. Shown are pooled data from three (S210C), two (S210C/F224C), two (S210C/Q216C), and two (wild type) biological replicates. Shown is the mean ± SEM.

B Movement type analysis of salivary gland-derived sporozoites (SGS) of the indicated parasite lines. *n* indicates the number of observed sporozoites. See Fig EV3 for the classification of different movement patterns. Floaters have been omitted in the analysis presented in the top graph and are not included in *n*. Shown are pooled data from three (S210C), three (S210C/Q216C) and two (wild-type) biological replicates. Shown is the mean ± SEM.

C Speed of hemolymph (HL)-derived productively gliding sporozoites from the indicated lines. Values (*n*) above dot plots indicate numbers of observed sporozoites. Data were tested for significance with Kruskal–Wallis test. Shown are pooled data from three (S210C), two (S210C/F224C), and two (wild-type) biological replicates.

D Percentage of gliding and non-gliding control hemolymph sporozoites (HLS) at increasing concentrations of DTT. *n* indicates the number of observed sporozoites. Floaters are included in the non-motile fraction. Each condition represents pooled data from two biological replicates. Shown is the mean ± SEM.

E Percentage of gliding hemolymph sporozoites (HLS) expressing the open TRAP I domain at increasing concentrations of DTT. *n* indicates the total number of observed sporozoites. Floaters are included in the nonmotile fraction. Shown are pooled data from three (0 mM DTT), two (50 mM DTT), and three biological replicates for concentrations of 100 mM DTT in the S210C/Q216C line. For concentrations of 200 mM and 330 mM DTT in the S210C/Q216C line, data shown represent pooled data from one biological replicate. Several comparable screening experiments previously performed showed no productive motility at these concentrations. Shown is the mean ± SEM.

F Maximum projections (1 min time lapse, 3 s per frame) of single *S210C/Q216C* sporozoites in the presence or absence of 50 mM DTT. A projection from a motile sporozoite of the *cFluo* line treated with 50 mM DTT is shown as control. Scale bar: 5 µm.

Source data are available online for this figure.

using these conditions motility was rescued to approximately 20–30% of wild-type level. While DTT clearly does not only act on TRAP, these data nevertheless suggest that DTT can reduce the introduced disulfide bond and enable some TRAP molecules on the sporozoite surface to function normally leading to an increase of migrating sporozoites.

The transition from a closed to an open state was suggested to be important based (i) on structural studies that revealed the I domain of *P. falciparum* and *P. vivax* TRAP in the closed and open conformations, respectively (Song *et al*, 2012) and (ii) analogy to the mechanism of action of I domains in human integrins (Shimaoka *et al*, 2003). In a closed state, the integrin I domain has a low affinity for ligand binding, which is greatly increased in the open state. Thus, a ligand-bound "open" TRAP might signal back to the cytoplasm to change the state of actin filament assembly or TRAP association with actin filaments (Song *et al*, 2012; Quadt *et al*, 2016). By stabilizing the closed or open state with disulfide bonds, we found that both parasite lines expressing these variants are severely compromised in their capacity to transmit from mosquitoes to mice. While not providing final proof, this phenotype indicates that a key feature of TRAP function during gliding and invasion is the dynamic interchange between a closed and an open conformation of the I domain.

### Conformational changes in sporozoite surface proteins and implications for vaccine design

Conformational changes have also been reported for the major surface protein, the GPI-anchored circumsporozoite protein CSP (Coppi *et al*, 2011; Herrera *et al*, 2015). Here, the N terminus appears to

**Table 3. Screening for TCEP and DTT concentrations affecting wild-type motility. ++ +: wild-type-like motility in the absence of drug, ++: 20–30% reduction from wild-type motility; +: 30–90% reduction compared with wild-type motility. –: no motility.**

| Parasite line | Reducing agent | Concentration (mM) | Incubation time (min) | Gliding capacity |
|---|---|---|---|---|
| cFluo | DTT | 0 | 15 | ++ + |
| | | 50 | 15 | ++ |
| | | 100 | 15 | + |
| | | 200 | 15 | + |
| | | 300 | 15 | – |
| | | 500 | 15 | – |
| | | 1,000 | 15 | – |
| cFluo | TCEP | 0 | 15 | ++ + |
| | | 5 | 15 | ++ |
| | | 10 | 15 | + |
| | | 20 | 15 | + |
| | | 50 | 15 | – |
| | | 100 | 15 | – |
| | | 200 | 15 | – |

**Table 4. Incubation of open I domain expressing sporozoites (*S210C/Q216C*) with DTT but not TCEP rescues motility. +: 30–90% reduction compared with wild-type motility. –: no motility.**

| Parasite line | Reducing agent | Concentration (mM) | Incubation time (min) | Gliding capacity |
|---|---|---|---|---|
| S210C/Q216C | DTT | 5 | 15 | – |
| | | 30 | 2 | – |
| | | 30 | 15 | – |
| | | 50 | 15 | + |
| | | 100 | 2 | – |
| | | 100 | 15 | + |
| | | 100 | 45 | – |
| | | 200 | 15 | – |
| | | 330 | 15 | – |
| S210C/Q216C | TCEP | 1 | 15 | – |
| | | 2 | 60 | – |
| | | 5 | 15 | – |
| | | 10 | 2 | – |
| | | 10 | 15 | – |
| | | 20 | 15 | – |
| | | 100 | 15 | – |

shield the single TSR of CSP and hence avoids critical ligand binding via the TSR until necessary. Yet, in CSP the N terminus is cleaved off by a protease, and hence, the protein might not undergo conformational change *per se*. TRAP shedding after cleavage by rhomboid proteases in its transmembrane domain is also important for gliding (Ejigiri *et al*, 2012). Several proteins have been suggested to specifically bind to TRAP: fetuin-A, a hepatocyte-specific protein (Jethwaney *et al*, 2005), saglin, an *Anopheles* salivary gland protein (Ghosh *et al*, 2009), alpha-v-containing integrins (Dundas *et al*, 2018), and platelet-derived growth factor beta (Steel *et al*, 2021). We have previously called into question the specificity of these interactions by reporting that an I domain from *Toxoplasma gondii* MIC2, and to a lesser extent from the human integrin αXβ2, can functionally replace the I domain of *Plasmodium berghei* TRAP (Klug *et al*, 2020). In analogy to certain human I domains such as αXβ2 and αMβ2 with promiscuous ligand binding (Springer, 2006), we interpreted these results to suggest that TRAP evolved to bind multiple ligands. Our current data cannot resolve this controversy, but we suggest that future efforts to screen for TRAP ligands might benefit from TRAP domains that are stabilized in the open and closed states.

Antibodies against sporozoite surface proteins, especially CSP, are being explored for passive immunization and to inform the improvement of CSP-based vaccines (Aliprandini *et al*, 2018; Julien & Wardemann, 2019; Murugan *et al*, 2020; Flores-Garcia *et al*, 2021; Gaudinski *et al*, 2021; Wang *et al*, 2021). CSP is the predominant antigen on the sporozoite surface with TRAP being among the most abundant other surface proteins. Yet, compared with CSP, most of the TRAP is stored in secretory micronemes and only a small proportion is exposed on the sporozoite surface (Carey *et al*, 2014; Kehrer *et al*, 2016). Antibodies against TRAP have been generated and probed for their capacity to inhibit sporozoite gliding. While a first report of such inhibitory capacity (Spaccapelo *et al*, 1997) could not be reproduced (Gantt *et al*, 2000), several studies explored TRAP as a vaccine candidate (Tiono *et al*, 2018; Kim *et al*, 2020; Lu *et al*, 2020; Nazeri *et al*, 2020). Our work suggests that antibodies that stabilize the conformation of the TRAP I domain in either the open or the closed state could contribute to stopping parasite migration in the skin or during liver entry.

### Implication of conformational changes for sporozoite gliding

Sporozoites glide in a stick–slip fashion by attaching to the substrate at distinct sites leading to slowing of motility (stick), while the release of some (but not all) adhesion sites leads to transiently faster movements (slip; Münter *et al*, 2009). The overall progress of sporozoites thus rests on a fine balance between adhesion and de-adhesion that is likely governed by the interplay of different proteins (Hegge *et al*, 2012), protein–ligand interactions (Perschmann *et al*, 2011) and protease activity (Ejigiri *et al*, 2012). Gliding motility is affected differently in the parasites expressing TRAP with the I domain fixed in the two states. The closed mutant (S210C/F224C) shows less adhesion and faster motility likely because of weakened adhesion capability or redundancy with other sporozoite adhesins (Fig 5A and C). The open mutant (S210C/Q216C) appears to have normal or even enhanced adhesion to the substrate yet does not move productively, suggesting that it cannot detach from the substrate. This could however also be based on possible differences in the trapping efficiency of the introduced disulfide bonds leading to a stronger stabilization of the open conformation in the S210C/Q216C mutant compared with the closed state in the S210C/F224C mutant. As a consequence, some TRAP

mutants might be partially able to transition between the open and closed states, enabling some movement, including faster movement by the mutant stabilized in the closed state. Still, the difference between the two mutants in their capability to move productively as well as the strong adhesion of salivary gland sporozoites expressing the open I domain (S210C/Q216C) indicates a difference in the ligand binding affinity as reported for human integrins with an I domain trapped in the open state (Shimaoka *et al*, 2003). This is also reminiscent of a mutant where TRAP cannot be cleaved by rhomboid proteases (Ejigiri *et al*, 2012). Rhomboid proteases cleave TRAP and hence ensure detachment from the substrate for efficient gliding motility. Mutations in TRAP that prevented cleavage by rhomboid proteases yielded sporozoites with severely compromised motility that struggled to enter salivary glands. The inability of sporozoites with the conformationally stabilized TRAP I domain to migrate suggests that sporozoites rely on both a dynamic conformational change in the I domain and rhomboid-mediated cleavage to ensure rapid gliding motility, which proceeds at a rate 10 times faster than rapidly migrating human cells such as neutrophils.

In conclusion, we suggest that the capacity of the TRAP I domain to dynamically switch between two conformational states is essential for *Plasmodium* sporozoite migration and transmission. Anti-TRAP antibodies that fix the I domain in one of the conformational states could constitute new tools to prevent malaria infection alone or in combination with anti-CSP antibodies.

## Materials and Methods

### Reagents and Tools table

| Reagent/resource | Reference or source | Identifier or catalog number |
|---|---|---|
| CD-1 (*Mus musculus*) | Janvier Labs/Charles River Laboratories | N/A |
| C57BL/6JRj (*Mus musculus*) | Janvier Labs/Charles River Laboratories | N/A |
| XL1-blue cells (*Escherichia coli*) | Agilent Technologies | Cat # 200236 |
| *trap(-)* (*Plasmodium berghei*) | Klug *et al* (2020) | N/A |
| *cfluo* (*Plasmodium berghei*) | Klug *et al* (2020) | N/A |
| *S210C* (*Plasmodium berghei*) | This study | N/A |
| *S210C/Q216C* (*Plasmodium berghei*) | This study | N/A |
| *S210C/F224C* (*Plasmodium berghei*) | This study | N/A |
| **Antibodies** | | |
| Mouse anti-CSP monoclonal | Yoshida *et al* (1980) | MR4: MRA-100 |
| Rabbit anti-TRAP polyclonal | Klug *et al* (2020) | N/A |
| Goat anti-rabbit HRP | Bio-Rad | Cat # 1705046 |
| Sheep anti-mouse HRP | Sigma-Aldrich | NXA931-1ML |
| Goat anti-rabbit Atto 647N polylconal | Sigma-Aldrich | Cat # 40839 |
| Goat anti-rabbit AlexaFluor488 polyclonal | ThermoFisher | Cat # A11008 |
| Goat anti-mouse Atto 594 polyclonal | Sigma-Aldrich | Cat # 76085 |
| **Oligonucleotides and other sequence-based reagents** | | |
| PCR primers | This study | Table EV1 |
| **Chemicals, enzymes and other reagents** | | |
| Hoechst 33342 | ThermoFisher | Cat # H3570 |
| TCEP-HCL | ThermoFisher | Cat # PG82080 |
| DTT | ThermoFisher | Cat # 20290 |
| **Software** | | |
| Prism 9.3.1 | https://www.graphpad.com/scientific-software/prism/ GraphPad | |
| AxioVision | https://www.zeiss.com/microscopy/int/home.html Carl Zeiss Microscopy | |
| ApE | https://jorgensen.biology.utah.edu/wayned/ape/ ApE – A plasmid Editor by M. Wayne Davis | |
| FIJI/ImageJ | https://imagej.net/software/fiji/ Schindelin *et al* (2012) | |

## Methods and Protocols

### Ethics statement

Animal experiments were performed according to the Federation of European Laboratory Animal Science Associations (FELASA) and Society of Laboratory Animal Science (GV-SOLAS) guidelines and approved by the responsible German authorities (Regierungspräsidium Karlsruhe). Mice were obtained from JANVIER or Charles River Laboratories and kept in the dedicated animal facility of Heidelberg University according to current guidelines (three mice per cage, *ad libitum* food and water, environmentally enriched cages). Mice were euthanized once symptoms of cerebral malaria appeared but latest at Day 10 after infection.

### Animal models

Female 4–6-week-old Swiss CD1 or C57BL/6 mice from Janvier or Charles River laboratories were used to propagate *P. berghei* parasites. Transgenic parasites were generated on the *Plasmodium berghei* ANKA strain (Vincke & Bafort, 1968) either directly in wild-type or wild-type-derived strains (e.g., *trap(−)* and *cFluo*). Parasites were cultured in Swiss CD1 mice, whereas transmission experiments with sporozoites were performed only in C57Bl/6 mice.

### Generation of *S210C*, *S210C/Q216C*, and *S210C/F224C* parasites

To generate the parasite lines *S210C*, *S210C/Q216C*, and *S210C/F224C*, we made use of a synthetic *trap* gene that had been codon modified for *E. coli* K12 and used previously to create I domain exchange mutants (Klug *et al*, 2020). The synthetic *trap* gene cloned in the pMK-RQ vector (Invitrogen) was targeted by site-directed mutagenesis using the primers P1149/P1150 (S210C), P1153/P1154 (Q216C), and P1151/P1152 (F224C; Table EV1). S210C/Q216C and S210C/F224C mutations were introduced sequentially. Mutated sequences were cloned into the Pb238-TRAP-NdeI/PacI vector (*NdeI/PacI*), linearized (*ScaI-HF*), and transfected into *P. berghei* ANKA using standard protocols (Janse *et al*, 2006). Isogenic parasite populations were generated as described previously (Klug *et al*, 2020).

### Mosquito infection

Mice were infected intraperitoneally by injection of frozen parasite aliquotes (~ 200–250 µl). Subsequently infected mice were bled by cardiac puncture once parasitemia reached ~ 2% and used for a fresh blood transfer of 20,000,000 parasites into each of two naïve mice. Mice that obtained a blood transfer were kept for further 3–4 days. Mice were fed to mosquitoes if at least three exflagellation events per field of view (as observed with a Zeiss Axiostar using a 100× objective lens revealing 300–400 red blood cells per field of view) were observed. Mice that contained the right density of gametocytes were anesthetized with a mixture of ketamine and xylazine (87.5 mg/kg ketamine and 12.5 mg/kg xylazine), placed on mosquito cages, and covered with paper tissues to dim the light and enhance mosquito biting. Mosquitoes were allowed to take a blood meal for 20–30 min on at least two mice per mosquito cage. Mosquitos were shaken off twice during this period to guarantee that most mosquitoes had the chance to suck blood. Subsequently infected mosquitoes were kept at 80% humidity and 21°C in a climate chamber. Mosquitoes determined to be infected had to be 3–7 days old and were starved overnight prior to blood feeding.

### Preparation of hemolymph, midgut, and salivary gland sporozoites

Sporozoites were isolated from midguts, hemolymph, and salivary glands of infected mosquitos between Day 12 and Day 22 post-infection. The timepoint for dissection was dependent on the planned experiments; midgut sporozoites were dissected between Days 12 and 15, hemolymph sporozoites between Days 15 and 16, and salivary gland sporozoites between Days 17 and 22 post-infection. For counting experiments, midguts and salivary glands of at least 10 mosquitoes were dissected in phosphate-buffered saline (PBS), the tissue was crushed with a pestle, and free sporozoites were counted using a Neubauer counting chamber. The counting chamber was loaded with 10 µl solution from the side, and sporozoites were allowed to settle for 5 min prior to counting. Sporozoites were counted using a light microscope (Carl Zeiss, Axiostar) and 400-fold magnification. To isolate hemolymph sporozoites, mosquitoes were anesthetized by cooling on ice for at least 10 min. Once mosquitoes were immobile the last segment of the abdomen was cut with a syringe. Prepared mosquitoes were flushed by inserting a long-drawn Pasteur pipette into the lateral side of the thorax and injected with Roswell Park Memorial Institute medium 1640 (RPMI; supplemented with 50,000 units/l penicillin and 50 mg/l streptomycin). The hemolymph was thus drained from the abdomen, collected on a piece of foil, and transferred to a plastic reaction tube (Eppendorf). Hemolymph (HL) sporozoites were counted as previously described for midgut and salivary gland sporozoites.

### Gliding assays under regular and reducing conditions

To reduce introduced disulfide bonds fixing the TRAP I domain in the open confirmation, a reducing agent was added prior to the gliding essay. HL sporozoites were dissected according to standard protocols. Samples were centrifuged for 1 min at 13,000 rpm (Thermo Fisher Scientific, Biofuge primo), and supernatant was removed and replaced with dithiothreitol (DTT) or tris(2-carboxyethyl)phosphine (TCEP) diluted in RPMI at various concentrations (DTT: 50–1,000 mM, TCEP: 5–200 mM) and incubated for varying lengths of time (2–60 min). Subsequently samples were centrifuged, and sporozoite pellets were washed three times with RPMI. Finally, after the last washing step, RPMI was replaced with RPMI containing 3% bovine serum albumin (BSA) to activate sporozoites and samples were transferred to a 96-well plate with optical bottom (Nunc). To allow sporozoites to attach, plates were centrifuged at 1,500 rpm for 3 min (Heraeus Multifuge S1). Fluorescence microscopy (Axiovert 200 M, Carl Zeiss) with a 25× objective was used to capture 1–3 min movies with a frame rate of 3 s. The movies were analyzed using the Manual Tracking plugin of ImageJ (Schindelin *et al*, 2012) to determine the speed and trajectories of the moving sporozoites (see Classification of Sporozoites, Fig EV3). For standard sporozoite gliding assays, the treatment with TCEP or DTT as well as following washing steps were omitted. Instead, sporozoites were directly activated with RPMI containing 3% BSA and imaged as described.

### Classification of sporozoite movement patterns

Movement is described as gliding if sporozoites travel at least one full circle in a 3-min time lapse. Unproductive but motile forms of gliding are patch gliding and waving. Patch gliding describes

sporozoites moving back and forth over a single adhesion site. In the maximum projection, patch gliding sporozoites show a haystack pattern. Waving sporozoites are attached at a single adhesion side, swinging around with the other end. Non-motile sporozoites can either be attached or free-floating in the medium. For visual examples, please see Fig EV3.

#### Infection by mosquito bites and sporozoite injections

To determine the transmission potential of the generated parasite lines, mice were infected by mosquito bites and sporozoite injections. To study native transmission, mosquitoes that had been infected 17–24 days before were screened for the presence of sporozoites visible as GFP-positive midguts, separated in cups of 10 each, and starved for 6–8 h. Subsequently naïve female C57Bl/6 mice were anesthetized by intraperitoneal injection of a mixture of ketamine and xylazine (87.5 mg/kg ketamine and 12.5 mg/kg xylazine). Subsequently anesthetized mice were placed with the ventral side on the prepared cups for approximately 20 min. Mosquitoes that had taken a blood meal were dissected afterward to determine sporozoite numbers within salivary glands and midguts. For the injection of hemolymph sporozoites, the hemolymph of mosquitoes that had been infected 13–16 days before was obtained as described previously. Sporozoites were counted in a Neubauer counting chamber and diluted with PBS to 10,000 hemolymph sporozoites per 100 µl. If sporozoite concentrations were too low, samples were centrifuged for 1 min at 10,000 rpm (Thermo Fisher Scientific, Biofuge primo). Subsequently, the excess of liquid was removed and sporozoites were resuspended in an appropriate volume to achieve the planned dilution. For the injection of salivary gland sporozoites, the salivary glands of mosquitoes that had been infected 17–24 days earlier were dissected in PBS. Sporozoites were released as described above and diluted with PBS to 10,000 salivary gland sporozoites per 100 µl. Sporozoite solutions were injected intravenously into the tail vein of naïve C57Bl/6 mice. The parasitemia of infected mice was monitored by daily blood smears from Day 3 up to Day 20 post-infection. In addition, the survival of infected mice was monitored up to 20 days. Blood smears were stained in Giemsa solution (Merck) and counted using a light microscope (Carl Zeiss, Axiostar) with a counting grid. The time difference between the infection and the observation of the first blood stage was determined as prepatency.

#### Antibodies

For immunofluorescence stainings and western blots, we made use of antibodies directed against the circumsporozoite protein (CSP) and the thrombospondin-related anonymous protein (TRAP). The anti-CSP antibody mAb 3D11 (Yoshida *et al*, 1980) was applied as unpurified culture supernatant of the corresponding hybridoma cell line (1:200 diluted for immunofluorescence assays and 1:1,000 diluted for western blots). TRAP antibodies were generated as described previously (Klug *et al*, 2020) and applied as 1:200 dilution in immunofluorescence stainings and as 1:1,000 dilution for western blots. Secondary antibodies coupled to AlexaFluor 488 (Goat anti-Rabbit), Atto647N (Goat anti-Rabbit), and Atto 594 (Goat anti-Mouse) were obtained from Thermo Fisher and Sigma-Aldrich and used as 1:200 dilution in immunofluorescence stainings to visualize localization of TRAP and CSP. To avoid spillover of fluorescence signals in *P. berghei* lines expressing mCherry at the sporozoite stage, Atto647N secondary antibodies were applied to visualize TRAP while CSP and TRAP in nonfluorescent *P. berghei* lines were stained using AlexaFluor488 and Atto594 secondary antibodies. For western blots, secondary antibodies coupled to HRP (Bio-Rad and GE Healthcare) at 1:10,000 dilution were applied (Sheep anti-Mouse, Goat anti-Rabbit).

#### Immunofluorescence staining

Localization of TRAP and CSP was visualized by immunofluorescence staining of hemolymph sporozoites. Hemolymph was isolated from *P. berghei*-infected mosquitoes as described previously (Klug *et al*, 2020) and collected in plastic reaction tubes. Obtained hemolymph sporozoites were transferred into an 8-well glass-bottom imaging chamber (Nunc Lab-Tek), activated with 3% BSA in RPMI medium, and forced to attach to the bottom by centrifugation at 800 rpm for 8 min. Subsequently sporozoites were allowed to glide for 15 min at RT. Afterwards, samples were fixed using 4% paraformaldehyde (PFA) in PBS for 1 h at room temperature (RT). Fixed samples were washed three times with PBS and treated with primary antibody solutions for 1 h at RT. Subsequently samples were washed three times with PBS and treated with secondary antibody solutions for 1 h at RT in the dark. Finally, samples were washed three times in PBS and the supernatant was discarded. Samples were examined directly using a spinning disc confocal microscope (Nikon Ti series) with 100-fold magnification (Plan Apo VC 100×/1.4 N.A. oil immersion) and a Hamamatsu sCMOS ORCA Flash 4.0 camera.

#### Western blotting

Western blotting was performed as described in Klug *et al* (2020). Hemolymph sporozoites were isolated from infected mosquitoes by flushing with PBS using a drawn-out pipette as described before. Sporozoite solutions were kept on ice, counted using a hemocytometer, and distributed to 30,000 sporozoites per reaction tube. Samples were centrifuged for 1 min with 13,000 rpm (Thermo Fisher Scientific, Biofuge primo) at 4°C to pellet sporozoites. Subsequently, the supernatant was discarded and pellets were lysed in 20 µl RIPA buffer (50 mM Tris pH 8, 1% NP40, 0.5% sodium deoxycholate, 0.1% SDS, 150 mM NaCl, 2 mM EDTA) supplemented with protease inhibitors (Sigma-Aldrich, P8340) for ≥ 1 h on ice. Lysates were mixed with Laemmli buffer, heated for 10 min at 95°C, and centrifuged for 1 min at 13,000 rpm (Thermo Fisher Scientific, Biofuge primo). Samples were separated on precast 4–15% SDS–PAGE gels (Mini Protein TGX Gels, Bio-Rad) and blotted on nitrocellulose membranes with the Trans-Blot Turbo Transfer System (Bio-Rad). Blocking was performed by incubation in PBS containing 0.05% Tween20 and 5% milk powder for 1 h at RT. Afterward the solution was refreshed and antibodies directed against TRAP (rabbit polyclonal antibody, 1:1,000 diluted) or the loading control CSP (mAb 3D11, cell culture supernatant 1:1,000 diluted) were added. Membranes were washed three times (PBS with 0.05% Tween20), and secondary anti-rabbit antibodies (Immun-Star (GAR)-HRP, Bio-Rad) or anti-mouse antibodies (NXA931, GE Healthcare), conjugated to horse radish peroxidase, were applied for 1 h (1:10,000 dilution) at room temperature. Signals were detected using SuperSignal West Pico Chemiluminescent Substrate or SuperSignal West Femto Maximum Sensitivity Substrate (Thermo Fisher Scientific). After the detection of TRAP, blots were treated with stripping buffer (Glycine 15 g/l, SDS 1 g/l,

Tween20 10 ml/l, pH 2,2) for 15 min prior to incubation with anti-CSP antibodies used as loading control.

#### *AlphaFold prediction*

Models were predicted using AlphaFold2 Colab (Mirdita *et al*, 2022) https://colab.research.google.com/github/sokrypton/ColabFold/blob/main/beta/AlphaFold2_advanced.ipynb. Predicted structures have been uploaded to Zenodo, accession code 7613487 with https://doi.org/10.5281/zenodo.7613487.

#### *Statistical analysis*

Statistical analysis was performed using GraphPad Prism 9.3.1 (GraphPad, San Diego, CA, USA). Datasets were either tested with a one-way ANOVA (Kruskal–Wallis test) or a Student's *t*-test. A value of $P < 0.05$ was considered significant. Experiments have not been blinded.

## Data availability

All data have been made available in the manuscript. This study includes no data deposited in external repositories.

**Expanded View** for this article is available online.


### Acknowledgments

We thank Miriam Reinig and other members of the Frischknecht laboratory for mosquito rearing, Chafen Lu for discussions, and Franziska Hentzschel for comments on the manuscript. This project was funded by the Deutsche Forschungsgemeinschaft (DFG, German Research Foundation)—project number 240245660—SFB 1129, NIH Grant HL 131729, and the European Research Council (ERC StG 281719). FB is a member of the medical doctoral school at Heidelberg University medical faculty. DK was funded by a DFG postdoctoral fellowship (KL 3251/1-1) and is an alumnus of the Heidelberg Biosciences International Graduate School (HBIGS). We acknowledge the microscopy support from the Infectious Diseases Imaging Platform (IDIP) at the Center for Integrative Infectious Disease Research. The funders had no role in study design, data collection, and interpretation, or the decision to submit the work for publication. Open Access funding enabled and organized by Projekt DEAL.


### Author contributions

**Friedrich Braumann:** Conceptualization; data curation; formal analysis; validation; investigation; visualization; methodology; writing – original draft; writing – review and editing. **Dennis Klug:** Conceptualization; data curation; formal analysis; supervision; investigation; visualization; methodology; writing – original draft; writing – review and editing. **Jessica Kehrer:** Formal analysis; supervision; validation; investigation; methodology; writing – review and editing. **Gaojie Song:** Resources; visualization; methodology. **Juan Feng:** Resources; visualization; methodology. **Timothy A Springer:** Conceptualization; software; formal analysis; supervision; funding acquisition; investigation; visualization; methodology; writing – original draft; writing – review and editing. **Friedrich Frischknecht:** Conceptualization; supervision; funding acquisition; writing – original draft; project administration; writing – review and editing.

### Disclosure and competing interests statement

The authors declare that they have no conflict of interest.

## References


Aliprandini E, Tavares J, Panatieri RH, Thiberge S, Yamamoto MM, Silvie O, Ishino T, Yuda M, Dartevelle S, Traincard F *et al* (2018) Cytotoxic anti-circumsporozoite antibodies target malaria sporozoites in the host skin. *Nat Microbiol* 3: 1224 – 1233

Bane KS, Lepper S, Kehrer J, Sattler JM, Singer M, Reinig M, Klug D, Heiss K, Baum J, Mueller AK *et al* (2016) The actin filament-binding protein coronin regulates motility in plasmodium sporozoites. *PLoS Pathog* 12: e1005710

Carey AF, Singer M, Bargieri D, Thiberge S, Frischknecht F, Ménard R, Amino R (2014) Calcium dynamics of plasmodium berghei sporozoite motility. *Cell Microbiol* 16: 768 – 783

Cline DJ, Redding SE, Brohawn SG, Psathas JN, Schneider JP, Thorpe C (2004) New water-soluble phosphines as reductants of peptide and protein disulfide bonds: reactivity and membrane permeability. *Biochemistry* 43: 15195 – 15203

Coppi A, Natarajan R, Pradel G, Bennett BL, James ER, Roggero MA, Corradin G, Persson C, Tewari R, Sinnis P (2011) The malaria circumsporozoite protein has two functional domains, each with distinct roles as sporozoites journey from mosquito to mammalian host. *J Exp Med* 208: 341 – 356

Doud MB, Koksal AC, Mi LZ, Song G, Lu C, Springer TA (2012) Unexpected fold in the circumsporozoite protein target of malaria vaccines. *Proc Natl Acad Sci USA* 109: 7817 – 7822

Douglas RG, Amino R, Sinnis P, Frischknecht F (2015) Active migration and passive transport of malaria parasites. *Trends Parasitol* 31: 357 – 362

Dundas K, Shears MJ, Sun Y, Hopp CS, Crosnier C, Metcalf T, Girling G, Sinnis P, Billker O, Wright GJ (2018) Alpha-v-containing integrins are host receptors for the plasmodium falciparum sporozoite surface protein, TRAP. *Proc Natl Acad Sci USA* 115: 4477 – 4482

Ejigiri I, Ragheb DR, Pino P, Coppi A, Bennett BL, Soldati-Favre D, Sinnis P (2012) Shedding of TRAP by a rhomboid protease from the malaria sporozoite surface is essential for gliding motility and sporozoite infectivity. *PLoS Pathog* 8: e1002725

Flores-Garcia Y, Wang LT, Park M, Asady B, Idris AH, Kisalu NK, Munoz C, Pereira LS, Francica JR, Seder RA *et al* (2021) The P. falciparum CSP repeat region contains three distinct epitopes required for protection by antibodies *in vivo*. *PLoS Pathog* 17: e1010042

Frischknecht F, Matuschewski K (2017) *Plasmodium* sporozoite biology. *Cold Spring Harb Perspect Med* 7: a025478

Gantt S, Persson C, Rose K, Birkett AJ, Abagyan R, Nussenzweig V (2000) Antibodies against thrombospondin-related anonymous protein do not inhibit plasmodium sporozoite infectivity *in vivo*. *Infect Immun* 68: 3667 – 3673

Gaudinski MR, Berkowitz NM, Idris AH, Coates EE, Holman LA, Mendoza F, Gordon IJ, Plummer SH, Trofymenko O, Hu Z *et al* (2021) A monoclonal antibody for malaria prevention. *N Engl J Med* 385: 803 – 814

Ghosh AK, Devenport M, Jethwaney D, Kalume DE, Pandey A, Anderson VE, Sultan AA, Kumar N, Jacobs-Lorena M (2009) Malaria parasite invasion of the mosquito salivary gland requires interaction between the plasmodium TRAP and the anopheles saglin proteins. *PLoS Pathog* 5: e1000265

Hegge S, Uhrig K, Streichfuss M, Kynast-Wolf G, Matuschewski K, Spatz JP, Frischknecht F (2012) Direct manipulation of malaria parasites with optical tweezers reveals distinct functions of plasmodium surface proteins. *ACS Nano* 6: 4648 – 4662

Heintzelman MB (2015) Gliding motility in apicomplexan parasites. *Semin Cell Dev Biol* 46: 135 – 142

Herrera R, Anderson C, Kumar K, Molina-Cruz A, Nguyen V, Burkhardt M, Reiter K, Shimp R Jr, Howard RF, Srinivasan P *et al* (2015) Reversible conformational change in the plasmodium falciparum circumsporozoite protein masks its adhesion domains. *Infect Immun* 83: 3771 – 3780

Hopp CS, Kanatani S, Archer NK, Miller RJ, Liu H, Chiou KK, Miller LS, Sinnis P (2021) Comparative intravital imaging of human and rodent malaria sporozoites reveals the skin is not a species-specific barrier. *EMBO Mol Med* 13: e11796

Janse CJ, Franke-Fayard B, Mair GR, Ramesar J, Thiel C, Engelmann S, Matuschewski K, van Gemert GJ, Sauerwein RW, Waters AP (2006) High efficiency transfection of plasmodium berghei facilitates novel selection procedures. *Mol Biochem Parasitol* 145: 60 – 70

Jethwaney D, Lepore T, Hassan S, Mello K, Rangarajan R, Jahnen-Dechent W, Wirth D, Sultan AA (2005) Fetuin-a, a hepatocyte-specific protein that binds plasmodium berghei thrombospondin-related adhesive protein: a potential role in infectivity. *Infect Immun* 73: 5883 – 5891

Julien JP, Wardemann H (2019) Antibodies against *Plasmodium falciparum* malaria at the molecular level. *Nat Rev Immunol* 19: 761 – 775

Kehrer J, Singer M, Lemgruber L, Silva PA, Frischknecht F, Mair GR (2016) A putative small solute transporter is responsible for the secretion of G377 and TRAP-containing secretory vesicles during plasmodium gamete egress and sporozoite motility. *PLoS Pathog* 12: e1005734

Kim YC, Dema B, Rodriguez-Garcia R, Lopez-Camacho C, Leoratti FMS, Lall A, Remarque EJ, Kocken CHM, Reyes-Sandoval A (2020) Evaluation of chimpanzee adenovirus and MVA expressing TRAP and CSP from plasmodium cynomolgi to prevent malaria relapse in nonhuman primates. *Vaccines (Basel)* 8: 363

Klug D, Goellner S, Kehrer J, Sattler J, Strauss L, Singer M, Lu C, Springer TA, Frischknecht F (2020) Evolutionarily distant I domains can functionally replace the essential ligand-binding domain of plasmodium TRAP. *Elife* 9: e57572

Li J, Springer TA (2017) Integrin extension enables ultrasensitive regulation by cytoskeletal force. *Proc Natl Acad Sci USA* 114: 4685 – 4690

Lu C, Song G, Beale K, Yan J, Garst E, Feng J, Lund E, Catteruccia F, Springer TA (2020) Design and assessment of TRAP-CSP fusion antigens as effective malaria vaccines. *PLoS One* 15: e0216260

Matuschewski K, Nunes AC, Nussenzweig V, Menard R (2002) *Plasmodium* sporozoite invasion into insect and mammalian cells is directed by the same dual binding system. *EMBO J* 21: 1597 – 1606

Menard R, Tavares J, Cockburn I, Markus M, Zavala F, Amino R (2013) Looking under the skin: the first steps in malarial infection and immunity. *Nat Rev Microbiol* 11: 701 – 712

Mirdita M, Schutze K, Moriwaki Y, Heo L, Ovchinnikov S, Steinegger M (2022) ColabFold: making protein folding accessible to all. *Nat Methods* 19: 679 – 682

Münter S, Sabass B, Selhuber-Unkel C, Kudryashev M, Hegge S, Engel U, Spatz JP, Matuschewski K, Schwarz US, Frischknecht F (2009) *Plasmodium* sporozoite motility is modulated by the turnover of discrete adhesion sites. *Cell Host Microbe* 6: 551 – 562

Murugan R, Scally SW, Costa G, Mustafa G, Thai E, Decker T, Bosch A, Prieto K, Levashina EA, Julien JP *et al* (2020) Evolution of protective human antibodies against plasmodium falciparum circumsporozoite protein repeat motifs. *Nat Med* 26: 1135 – 1145

Nazeri S, Zakeri S, Mehrizi AA, Sardari S, Djadid ND (2020) Measuring of IgG2c isotype instead of IgG2a in immunized C57BL/6 mice with plasmodium vivax TRAP as a subunit vaccine candidate in order to correct interpretation of Th1 versus Th2 immune response. *Exp Parasitol* 216: 107944

Perschmann N, Hellmann JK, Frischknecht F, Spatz JP (2011) Induction of malaria parasite migration by synthetically tunable microenvironments. *Nano Lett* 11: 4468 – 4474

Prudencio M, Rodriguez A, Mota MM (2006) The silent path to thousands of merozoites: the plasmodium liver stage. *Nat Rev Microbiol* 4: 849 – 856

Quadt KA, Streichfuss M, Moreau CA, Spatz JP, Frischknecht F (2016) Coupling of retrograde flow to force production during malaria parasite migration. *ACS Nano* 10: 2091 – 2102

Schindelin J, Arganda-Carreras I, Frise E, Kaynig V, Longair M, Pietzsch T, Preibisch S, Rueden C, Saalfeld S, Schmid B *et al* (2012) Fiji: an open-source platform for biological-image analysis. *Nat Methods* 9: 676 – 682

Shimaoka M, Lu C, Palframan RT, von Andrian UH, McCormack A, Takagi J, Springer TA (2001) Reversibly locking a protein fold in an active conformation with a disulfide bond: integrin alphaL I domains with high affinity and antagonist activity *in vivo*. *Proc Natl Acad Sci USA* 98: 6009 – 6014

Shimaoka M, Takagi J, Springer TA (2002) Conformational regulation of integrin structure and function. *Annu Rev Biophys Biomol Struct* 31: 485 – 516

Shimaoka M, Xiao T, Liu JH, Yang Y, Dong Y, Jun CD, McCormack A, Zhang R, Joachimiak A, Takagi J *et al* (2003) Structures of the alpha L I domain and its complex with ICAM-1 reveal a shape-shifting pathway for integrin regulation. *Cell* 112: 99 – 111

Song G, Koksal AC, Lu C, Springer TA (2012) Shape change in the receptor for gliding motility in plasmodium sporozoites. *Proc Natl Acad Sci USA* 109: 21420 – 21425

Spaccapelo R, Naitza S, Robson KJ, Crisanti A (1997) Thrombospondin-related adhesive protein (TRAP) of plasmodium berghei and parasite motility. *Lancet* 350: 335

Springer TA (2006) Complement and the multifaceted functions of VWA and integrin I domains. *Structure* 14: 1611 – 1616

Steel RWJ, Vigdorovich V, Dambrauskas N, Wilder BK, Arredondo SA, Goswami D, Kumar S, Carbonetti S, Swearingen KE, Nguyen T *et al* (2021) Platelet derived growth factor receptor beta (PDGFRbeta) is a host receptor for the human malaria parasite adhesin TRAP. *Sci Rep* 11: 11328

Sultan AA, Thathy V, Frevert U, Robson KJ, Crisanti A, Nussenzweig V, Nussenzweig RS, Menard R (1997) TRAP is necessary for gliding motility and infectivity of plasmodium sporozoites. *Cell* 90: 511 – 522

Tiono AB, Nebie I, Anagnostou N, Coulibaly AS, Bowyer G, Lam E, Bougouma EC, Ouedraogo A, Yaro JBB, Barry A *et al* (2018) First field efficacy trial of the ChAd63 MVA ME-TRAP vectored malaria vaccine candidate in 5-17 months old infants and children. *PLoS One* 13: e0208328

Vanderberg JP (1974) Studies on the motility of plasmodium sporozoites. *J Protozool* 21: 527 – 537

Vincke IH, Bafort J (1968) Standardization of the inoculum of plasmodium berghei sporozoites. *Ann Soc Belges Med Trop Parasitol Mycol* 48: 181 – 194

Wang LT, Pereira LS, Kiyuka PK, Schon A, Kisalu NK, Vistein R, Dillon M, Bonilla BG, Molina-Cruz A, Barillas-Mury C *et al* (2021) Protective effects of combining monoclonal antibodies and vaccines against the *Plasmodium falciparum* circumsporozoite protein. *PLoS Pathog* 17: e1010133

 

Yang M, Dutta C, Tiwari A (2015) Disulfide-bond scrambling promotes amorphous aggregates in lysozyme and bovine serum albumin. *J Phys Chem B* 119: 3969 – 3981

Yoshida N, Nussenzweig RS, Potocnjak P, Nussenzweig V, Aikawa M (1980) Hybridoma produces protective antibodies directed against the sporozoite stage of malaria parasite. *Science* 207: 71 – 73

# Expanded View Figures

**Figure EV1. AlphaFold predicted TRAP I domains and their reliability.**

A–D Predicted local-distance difference test (pLDDT) values plotted by sequence (A, B) and on the structures (C, D). (A, B) The pLDDT score for the models. (C, D) Ribbon cartoon models of the mutant I domains with predicted disulfide bonds shown in stick.

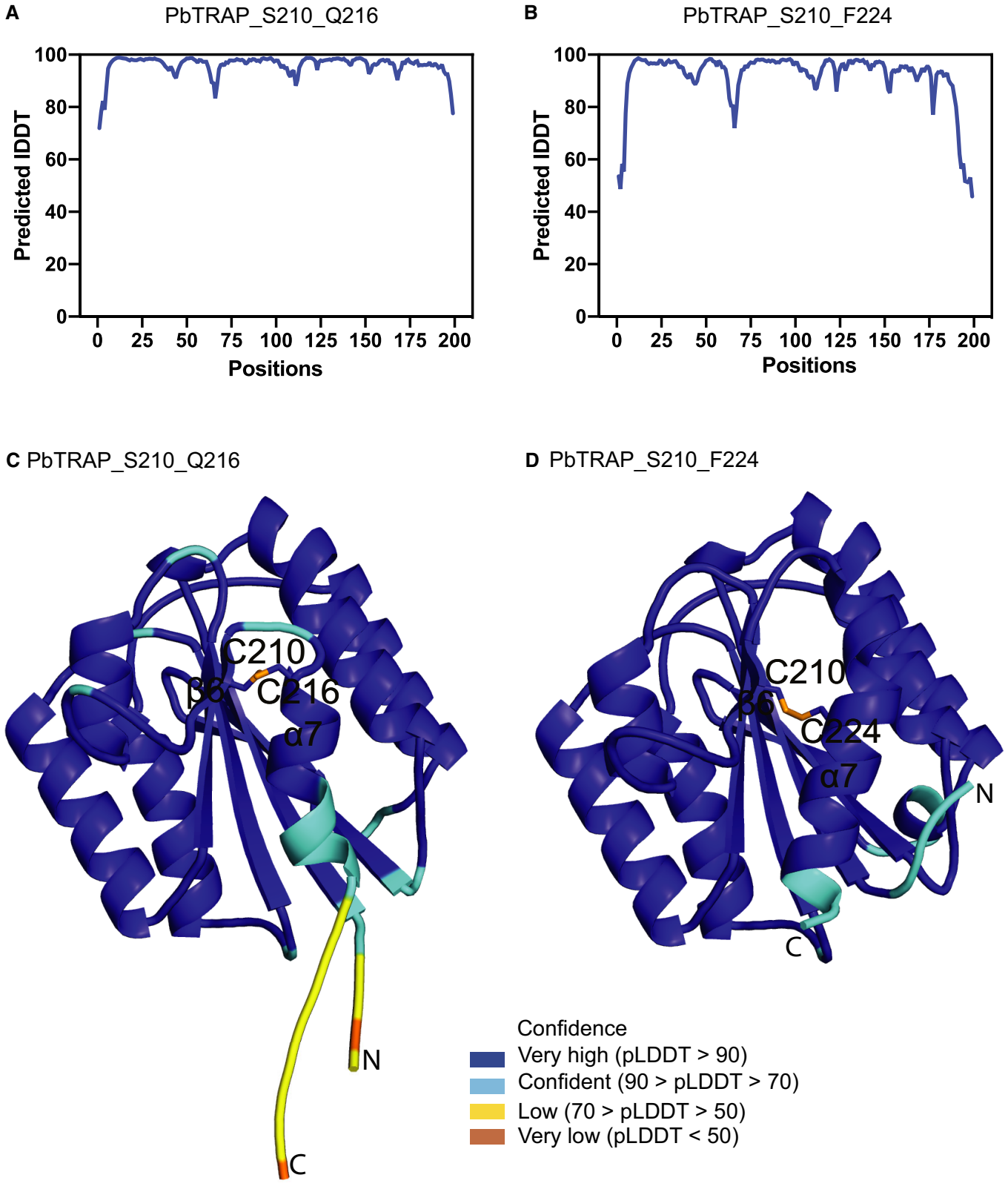


**Figure EV1.**

**Figure EV2. Generation of the recombinant parasite lines.**

A–D (A, C) TRAP genes with mutated I domains were transfected in *cFluo* or *trap(−)* parasites. Three different parasite lines were generated: *S210C*; control line with only one introduced cysteine, *S210C/Q216C*; mutant with two introduced cysteines which form a disulfide bond that stabilizes the I domain in the open" conformation and *S210C/F224C*; mutant with two introduced cysteines which form a disulfide bond that stabilizes the I domain in the "closed" conformation. The TRAP gene in all three generated lines was codon modified for *E. coli* K12. Binding sites of primers used for genotyping and lengths of PCR products are indicated below the scheme. Note that the illustration is not drawn to scale. (B, D) To control for correct integration of the transfected DNA sequences, three different PCRs were performed amplifying sequences that are specific for successful DNA integration at the 5′ (5′INT) and the 3′ (3′INT) end as well as a PCR that is specific for the recipient line (Control/Con or Knockout/KO). The lengths of the expected PCR products are depicted below the images. Shown are only PCR results of isogenic populations cloned by limiting dilution. To ensure the correct replacement of the native TRAP gene, the integration site of transfected parasites was sequenced.

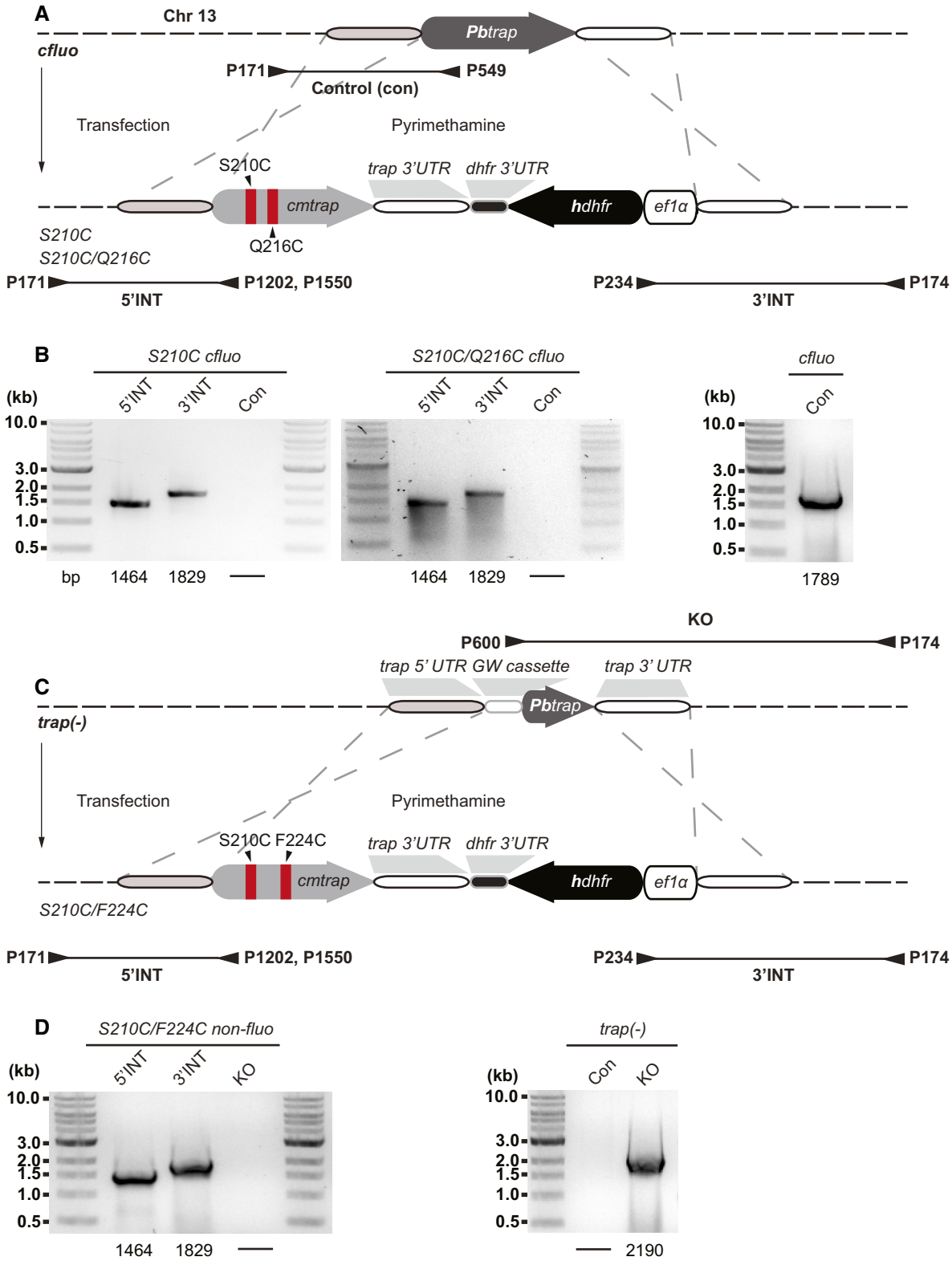


**Figure EV2.**

**Figure EV3. Movement patterns of *P. berghei sporozoites.***

Observed sporozoite movement patterns from movies with stills taken every 18 s. Right image shows maximum fluorescence projection. Active movement can be divided into productive gliding motility (top row, a) and unproductive movements such as lazy gliding for sporozoites gliding extremely slow (b), patch gliding for sporozoites moving rapidly over a single adhesion site in a back-and-forth manner (c), waving for sporozoites attached with one end and moving the rest of the sporozoite body within the medium (d). Nonmotile sporozoites can be either attached to the substrate (e) or floating in the medium (f). Scale bars: 5 μm. Red italic lettering is used here to make reference to the corresponding movement patterns illustrated in panel A of Fig EV4.

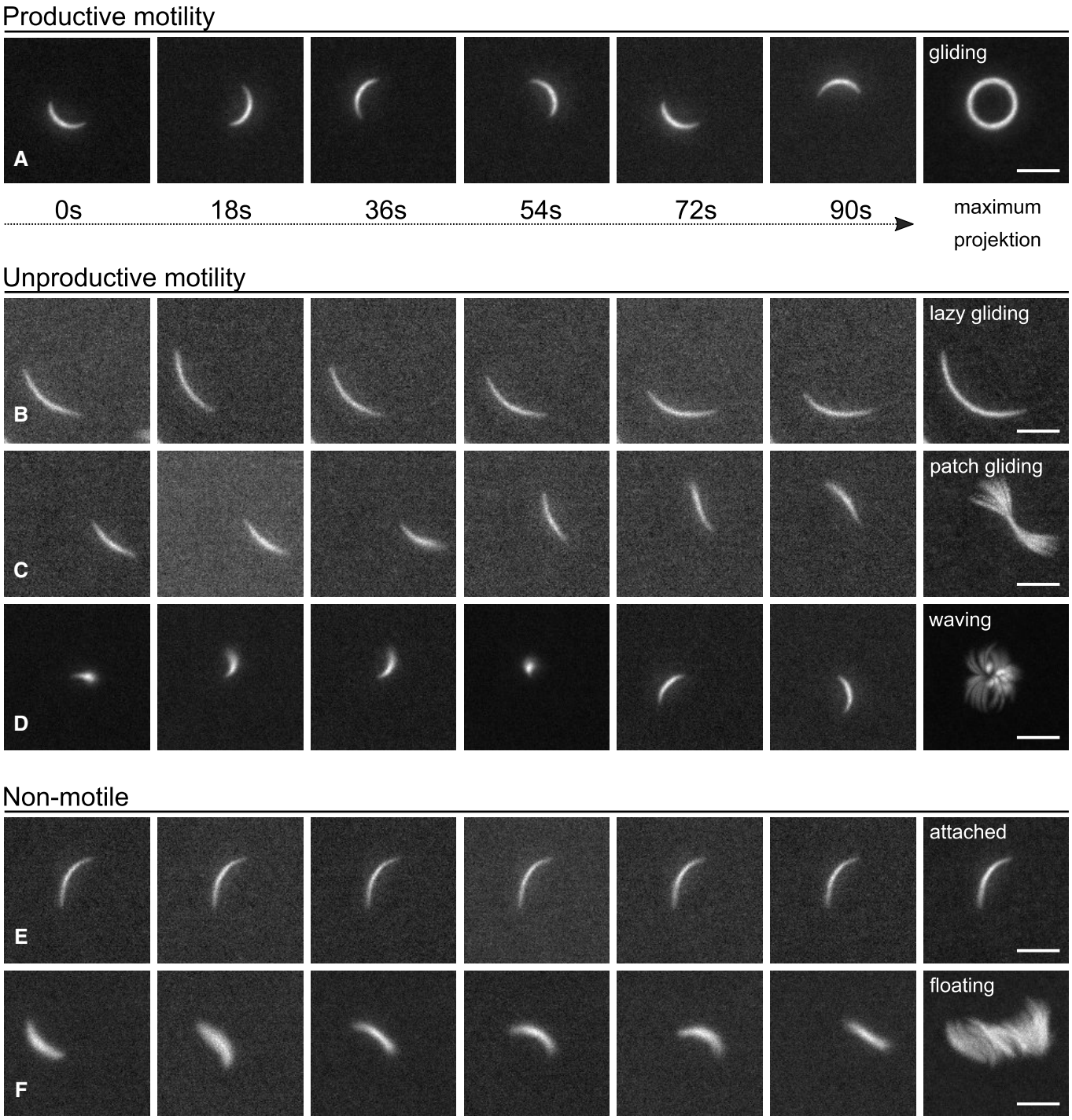


**Figure EV3.**

**Figure EV4. Reducing disulfide bonds with DTT rescues motility of sporozoites expressing the open I domain.**

A Sporozoites do not show movement at high concentrations of DTT. Top: still images of hemolymph sporozoites of the S210C line, S210C/Q216C line, and S210C/Q216C line treated with 330 mM DTT. Bottom: Maximum projections of movies for the same lines. Circular movement pattern (a) indicates productively moving sporozoites. For the open conformation, patch gliding sporozoites (haystack pattern, c) can be observed if no DTT is added. At a concentration of 330 mM DTT, only floating sporozoites (f) can be observed. In the bottom row, zoom-ins show sample sporozoites categorized into different movement patterns according to Fig EV3 (red lettering, d, waving). Scale bar: 30 μm.

B DTT rescues productive gliding in the open conformation. Gliding vs. non-gliding hemolymph sporozoites (HLS) of all lines. Floaters have been included for all lines. Note that the data for DTT treatment are also shown in Fig 5D and E and reproduced here together with the direct controls.

C Analysis of movement pattern of hemolymph-derived sporozoites (HLS) of the indicated parasite lines with (top) and without floaters (bottom). See Fig EV3 for the classification of different movement patterns. Floaters have been omitted for the lower graph.

D Movement type analysis of hemolymph-derived sporozoites (HLS) of the indicated parasite lines without floaters. Shown results represent the same datasets as in (B) and (C) in a combined manner and broken down by movement patterns. Note that sporozoites treated with DTT (including the 0 mM DTT control) have gone through an additional incubation and washing step. Floaters have been omitted. See Fig EV3 for the classification of different movement patterns.

Data information: In (B–D), shown are pooled data from three (0 mM DTT), two (50 mM DTT), and three biological replicates for concentrations of 100 mM DTT in the S210C/Q216C line. For concentrations of 200 and 330 mM DTT in the S210C/Q216C line, data shown represent pooled data from one biological replicate. Several comparable screening experiments previously performed showed no productive motility at these concentrations. Values (*n*) above plots in (B) indicate numbers of observed sporozoites. Shown is the mean ± SEM.

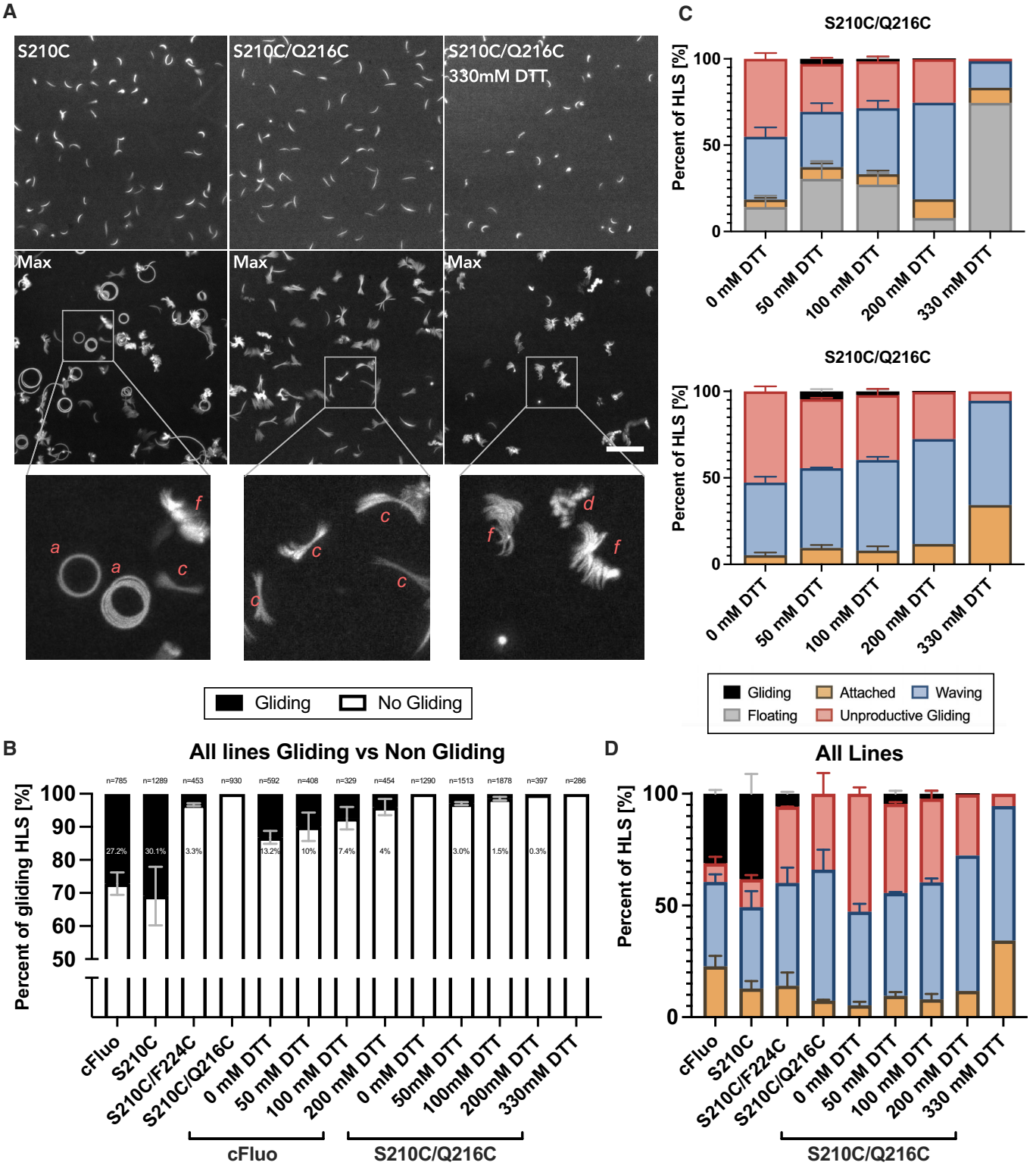


**Figure EV4.**